LETTERS

Local switching of two-dimensional superconductivity using the ferroelectric field effect

K. S. Takahashi[1], M. Gabay[2], D. Jaccard[1], K. Shibuya[3], T. Ohnishi[3], M. Lippmaa[3] & J.-M. Triscone[1]

Correlated oxides display a variety of extraordinary physical properties including high-temperature superconductivity[1] and colossal magnetoresistance[2]. In these materials, strong electronic correlations often lead to competing ground states that are sensitive to many parameters—in particular the doping level—so that complex phase diagrams are observed. A flexible way to explore the role of doping is to tune the electron or hole concentration with electric fields, as is done in standard semiconductor field effect transistors[3]. Here we demonstrate a model oxide system based on high-quality heterostructures in which the ferroelectric field effect approach can be studied. We use a single-crystal film of the perovskite superconductor Nb-doped $SrTiO_3$ as the superconducting channel and ferroelectric $Pb(Zr,Ti)O_3$ as the gate oxide. Atomic force microscopy is used to locally reverse the ferroelectric polarization, thus inducing large resistivity and carrier modulations, resulting in a clear shift in the superconducting critical temperature. Field-induced switching from the normal state to the (zero resistance) superconducting state was achieved at a well-defined temperature. This unique system could lead to a field of research in which devices are realized by locally defining in the same material superconducting and normal regions with 'perfect' interfaces, the interface being purely electronic. Using this approach, one could potentially design one-dimensional superconducting wires, superconducting rings and junctions, superconducting quantum interference devices (SQUIDs) or arrays of pinning centres.

Undoped perovskite $SrTiO_3$ is a band insulator. On chemical doping with oxygen, Nb or La ($SrTiO_{3-x}$, $SrTi_{1-x}Nb_xO_3$, $Sr_{1-x}La_xTiO_3$), the system undergoes a series of transitions from an insulating to a semiconducting state and, finally, to a metallic state. At low temperatures and at very low carrier densities between about 1×10^{19} and 10^{21} cm^{-3}, the system becomes superconducting[4–6]. Here, atomically flat Nb-doped $SrTiO_3$ films are used as an oxide superconductor. As $SrTiO_3$ is the 'natural' substrate for many perovskites, including ferroelectric $Pb(Zr,Ti)O_3$, single-crystal $Pb(Zr,Ti)O_3$ films can be grown on the Nb-doped $SrTiO_3$ films with a high degree of perfection. This allows us to explore the ferroelectric field effect approach[3,7,8] in this ideal low carrier density system. Epitaxial heterostructures composed of a 500-Å-thick layer of ferroelectric $Pb(Zr_{0.2}Ti_{0.8})O_3$ (PZT) and a 260-Å-thick layer of superconducting $Sr(Ti_{0.98}Nb_{0.02})O_3$ (Nb-STO) were fabricated on (001) $SrTiO_3$ (STO) single-crystal substrates. As schematically illustrated in Fig. 1a, standard photolithography and wet etching processes were used to pattern the devices in a geometry suitable for transport measurements. Experiments below 4.2 K and down to 30 mK were performed using a dilution refrigerator. The metallic tip of an atomic force microscope (AFM), acting as a mobile gate electrode, was used to sweep the entire area of the conducting path (the blue box region shown in Fig. 1a) at room temperature, causing a local switching of the direction of the ferroelectric polarization—parallel or anti-parallel to the *c* axis. The topographic image measured at the same time is shown in Fig. 1b. After the poling scan, AFM piezoresponse was used to determine the ferroelectric domain structure. A phase image, corresponding to a map of the material piezoelectric response is shown in Fig. 1c, revealing the two polarization states (P+ (dark red) and P− (light red)) and the artificially modified domain structure.

Figure 2a shows the temperature dependence of the resistivity for the two polarization states. The P+ state, poled using −12 V (on the tip), corresponds to the polarization direction that removes electrons from the Nb-STO layer. The P− state, poled using +12 V, corresponds to the polarization state that adds electrons to the Nb-STO layer, effectively increasing the doping level. Across the entire range of

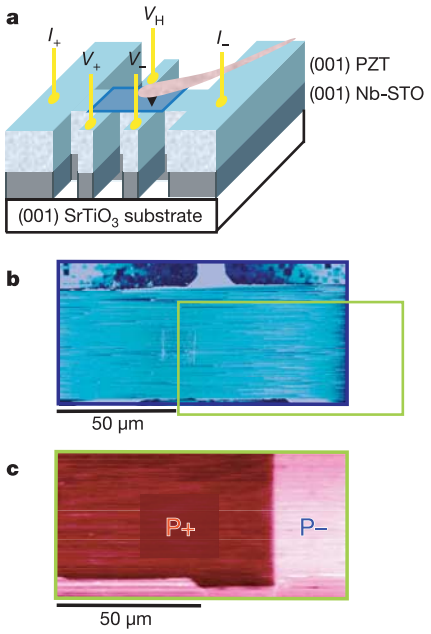

Figure 1 | Diagram of the device, and topographic and piezoelectric images of the field effect active region. a, Diagram of the device. The ferroelectric polarization was switched in the blue box area using the AFM tip as a local electrode, scanning the whole area. PZT, $Pb(Zr_{0.2}Ti_{0.8})O_3$; Nb-STO, $Sr(Ti_{0.98}Nb_{0.02})O_3$; V_H, V_+ and V_- are the voltage electrodes for Hall and resistivity measurements; I_+ and I_- are the current electrodes. **b**, AFM topographic image measured during the poling scan (120 μm × 60 μm). **c**, Piezoresponse image of the green rectangle area in **b** after poling from the P− state to the P+ state. (P+ corresponds to the polarization direction that removes electrons from the Nb-STO layer. In the P− state, the polarization field adds electrons to the film.)

[1]DPMC, University of Geneva, 24 Quai Ernest Ansermet, 1211 Geneva 4, Switzerland. [2]Laboratoire de Physique des Solides, Université de Paris-Sud, 91405 Orsay, France. [3]Institute for Solid State Physics, University of Tokyo, Chiba 277-8581, Japan.

our temperature scan, both states showed metallic behaviour and displayed large (field induced) resistance modulations. As expected from the electron-like conduction character of doped STO, the resistivity of the P− state is lower than that of the P+ state, as the field effect modulates the electron carrier density. At room temperature, a 60% difference between the two resistivity states was observed, and this value gradually decreased down to 20% as the temperature was reduced.

In order to investigate quantitatively the ferroelectric field effect carrier modulation, the Hall effect was measured for the two polarization states at various temperatures. Figure 2b shows the inverse Hall coefficient (R_H^{-1}) for the two states and the difference (ΔR_H^{-1}) as a function of temperature. As the field effect induces a carrier profile at the interface in the Nb-STO layer, the measured value of R_H^{-1} is somehow 'averaged' over the whole Nb-STO layer thickness (260 Å). The characteristic width of the carrier modulation length in a semiclassical metallic system is given by the Thomas–Fermi screening length: $\lambda_{TF} = (\varepsilon E_F/6\pi ne^2)^{1/2}$, where ε is the dielectric constant, E_F the Fermi energy, n the carrier density and e the electronic charge. For doped STO ($n = 5 \times 10^{19}\,cm^{-3}$, $E_F = 30$ meV), λ_{TF} at 300 K is ~30 Å and λ_{TF} below 5 K is ~210 Å, assuming that the temperature dependence of ε is similar to that of undoped single crystals[9]. From 260 K to 100 K, a very large, almost temperature independent, modulation of the Hall response (~60%) was observed, its size being comparable to that of the corresponding modulation in resistivity. Below 100 K, however, R_H^{-1} dramatically decreases for both polarization states. This behaviour is very different from the essentially temperature independent Hall coefficient observed in single crystals[10], making the large temperature dependence observed for ΔR_H^{-1} below 100 K very intriguing.

In a simple single band model, ΔR_H^{-1} would be proportional to the difference in carrier density (Δn), $\Delta n = \Delta P/ed$, where ΔP is the change in the PZT polarization and d is the thickness of the Nb-STO layer (260 Å). Because ΔP is essentially constant below 300 K (the ferroelectric Curie temperature of PZT being ~700 K), one would expect ΔR_H^{-1} to be constant[11]. Given that the Hall coefficient is temperature independent above 100 K and below 20 K, and that T_c (the superconducting critical temperature) versus doping thin film data (discussed later) can only be compared with single crystals using the high temperature Hall effect data, one could infer that the strong decrease in inverse Hall coefficient does not reflect carrier freezing but may rather be related to localization, band effects or multiband conduction. To determine the carrier densities n (calculated from $R_H^{-1} = en$), we have thus used the high temperature, T independent, inverse Hall coefficient. This gives us an average value of about $(4–5) \times 10^{19}\,cm^{-3}$ for the P+ state and of $7.5 \times 10^{19}\,cm^{-3}$ for the P− state. These values correspond to approximately 20% of active Nb sites, a fraction reasonably close to reports on thin films and single crystals[8,12,13]. Although the exact doping mechanism is unknown, Nb doping turned out to be very robust. Annealing at 500 °C only marginally changes the film conductivity, and experiments carried out over two years did not affect the properties of the devices. The measured change in carrier density implies a ΔP value of 10–14.5 $\mu C\,cm^{-2}$ ($P \approx 6\,\mu C\,cm^{-2}$). This value is of the order of the polarization field measured in similar devices, suggesting that the high temperature Hall coefficient yields a correct estimate of the carrier density.

Figure 3a shows the temperature dependence of the resistivity of each state below 380 mK. Both states display sharp superconducting transitions, reaching zero resistance, with a clear shift of the transition observed. With T_c defined as the temperature at which the

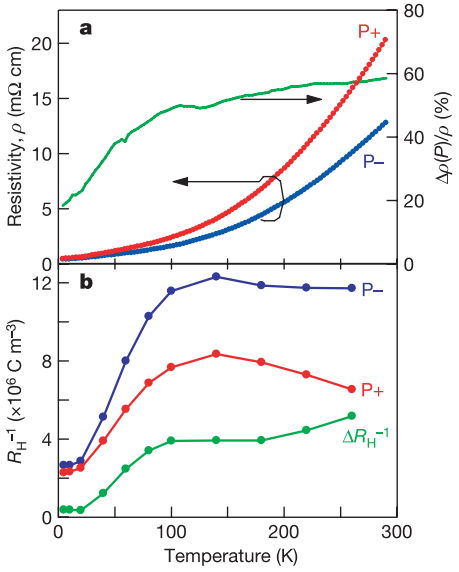

Figure 2 | Transport properties for the two polarization states. **a**, Left axis: temperature dependence of the resistivity (ρ) for the two polarization states, P+ and P−. Right axis (green curve): temperature dependence of the resistivity difference ratio between the two polarization states defined as $\Delta\rho(P)/\rho = (\rho\,(P+) - \rho(P-))/\rho(P-)$. **b**, Temperature dependence of the inverse Hall coefficient (R_H^{-1}) and the difference $\Delta R_H^{-1} = R_H^{-1}(P-) - R_H^{-1}(P+)$.

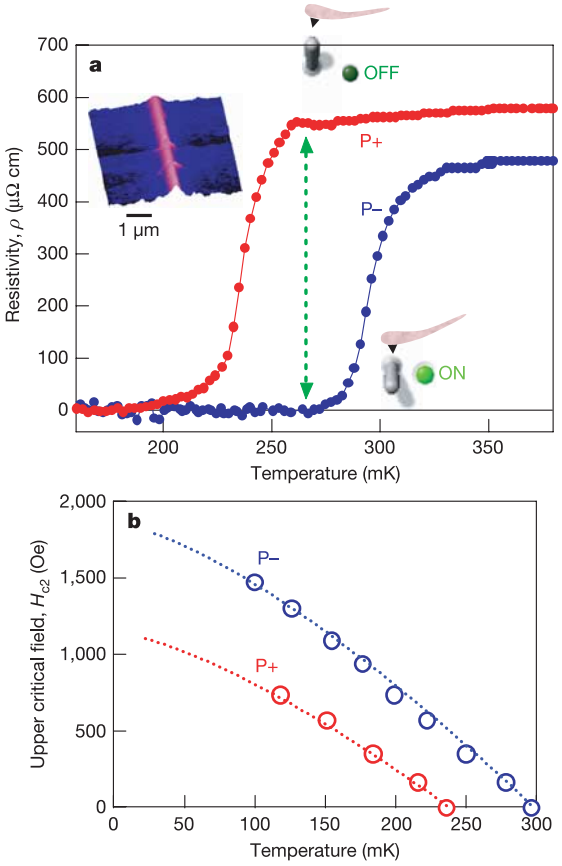

Figure 3 | Superconducting properties for the two polarization states. **a**, Resistivity versus temperature at low temperatures. As indicated by the arrow and the associated insets, a superconducting on-off switching is observed around 270 mK, illustrated by the 'AFM switch' shown as insets. The left inset shows the piezoresponse image after poling a P+ state line in the P− state background. **b**, Temperature dependence of the upper critical field, H_{c2}, for each state. $T_c(H)$ is defined as the temperature at which the resistivity decreases to 50% of the resistivity at 400 mK. Dotted lines indicate the WHH model fittings (see text).

resistivity decreases to 50% of the value at 400 mK, the T_c value for the P− state is 296 mK and that of the P+ state is 236 mK. Around 270 mK, the green arrow shows that switching of the ferroelectric polarization induces a transition from the normal state (P+ state) to a zero resistance superconducting state (P− state). In general, such a 'complete' switching is very difficult to obtain, because transitions to the superconducting state are often broad in very thin films (in fact broader than the induced shift of T_c). In high-T_c oxide films[14,15] and in ultrathin bismuth films[16], a field induced superconductor–insulator transition was however observed in few cases. The complete switching observed here is extremely promising for the promotion of the local ferroelectric field effect idea proposed in 1997 by Ahn *et al.*[7], and it could lead to novel nanoscale superconducting devices. As an example, the inset of Fig. 3a shows the piezoresponse image of part of the conducting path after AFM writing of a P+ domain line (red) in the P− background (blue).

Superconductivity is suppressed by applying a magnetic field along the [001] direction (out of the film plane). Figure 3b shows the upper critical field H_{c2} as a function of T. $T_c(H)$ is defined as the temperature at which the resistivity drops down to 50% of its value at 400 mK (we will justify this choice below). The temperature dependence of $H_{c2}(T)$ can be roughly fitted to the WHH model that describes conventional dirty limit type-II superconductors[17], in agreement with an estimation of ξ_0/l (∼30) ≫ 1, where ξ_0 is the BCS superconducting coherence length[19] and l the normal state mean free path. The estimated upper critical field at $T = 0$ is about 2,000 Oe for the P− state and 1,100 Oe for the P+ state, respectively. The superconducting coherence length can thus be calculated using $H_{c2}(0) = \Phi_0/2\pi\xi(0)^2$, where Φ_0 is the flux quantum and $\xi(0)$ is the coherence length at 0 K, which gives 400 Å for the P− state and 550 Å for the P+ state. If the scattering rate is taken to be the same for the P+ and P− states, the change in coherence length can be related to the changes in T_c, resistivity and Hall coefficient, leading to a 33% change as compared to the 40% experimentally observed. The fact that the coherence length is larger (for both polarization states) than the film thickness (260 Å) indicates that the superconducting system is two dimensional (2D).

The 2D nature of the superconducting transition can be confirmed by an analysis of paraconductivity fluctuations. Resistivity measurements with low noise level reveal that the resistivity starts to deviate slightly from the normal state T behaviour around 1.4 K with a temperature dependence that can be fitted to a 2D fluctuation model[18,19]. A fit of resistivity, ρ, versus T for the P+ and P− states allows us to determine the mean field critical temperature of each state. These values match closely the values of T_c obtained from the '50% of the normal state resistance' criterion, thus 'justifying' a posteriori our T_c determination and validating our H_{c2} analyses. Of course T_c plays the role of a mean field critical temperature as the actual zero field transition is expected to be Kosterlitz–Thouless (KT) like[20]. Fitting the tails of the resistive transitions yields estimates of the transition temperature T_{KT} and of the mean field T_c (ref. 21). For the P+ and the P− states we get T_{KT} values of 170 mK and 252 mK, and T_c values of 239 mK and 295 mK, respectively. Using Beasley *et al.*'s criterion[22] also allows T_{KT} and T_c to be determined. Making use of the relationship $T_{KT}/T_c = (1 + 0.173R_\square/(\hbar/e^2))^{-1}$ where $R_\square = \rho_N/d$ is the sheet resistance, ρ_N the normal state resistance and d the film thickness, one would conclude that $T_{KT} \approx T_c$ for the two states, which clearly disagrees with our findings.

Gabay *et al.* claimed[23] that the smallness of the core energy invalidates the standard KT scenario for most superconducting films, as it leads to large effective vortex dielectric constants, ε^*. Instead, they predicted the existence of a new vortex-antivortex lattice phase, which melts via a KT transition at a temperature T_{KT} sizably smaller than that derived by Beasley *et al.* Because the transition temperature is much less than T_c, the superfluid sheet density can be expected to approach its asymptotic zero temperature limit and T_{KT} should be proportional to the carrier sheet density so long as ε^* is not too strongly T dependent. This is illustrated in Fig. 4, which shows the dependence of the mean field (Fig. 4a) and KT transition temperatures (Fig. 4b) (determined above and listed in the figure legend) on carrier density n for the two states mapped onto the 'chemical doping' STO phase diagram. We identify the T_{KT} that we extracted from our resistivity curves with the melting temperature of the vortex-antivortex crystal. As can be seen in Fig. 4a and b, the T_c values for the two states fall reasonably well on the reduced STO curve, while T_{KT} is proportional to n as illustrated by the black dotted line. As the coherence length of superconducting Nb-STO is larger than d, although the change in carrier density is induced only near the Nb-STO/PZT interface, the Cooper pairs experience an average effective interaction through the proximity effect. We thus plot the average carrier densities calculated from the average R_H^{-1} in Fig. 4. Note that using the low temperature Hall coefficient values would lead to points that lie far off the single crystal curves. It is noteworthy that the field induced modulations of T_{KT} and T_c reflect different physics. T_{KT}, as explained above, is directly linked to the 2D superfluid density which is modified by the field effect. On the other hand, the electrostatic modulation of the mean field T_c is consistent with

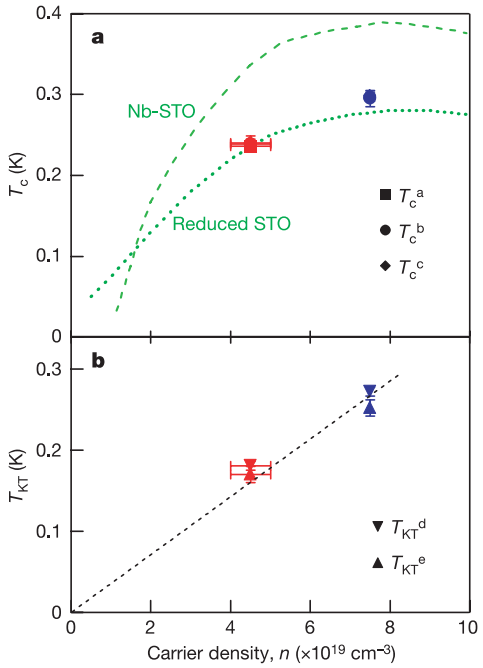

Figure 4 | Dependence of the critical temperature on carrier density for the two polarization states. a, The dependence of the mean field transition temperatures, T_c, on carrier density, n, for the two polarization states. The behaviour of reduced STO bulk crystals (green dotted line) and Nb-doped STO bulk crystals (green dashed line) are also included. **b**, The dependence of the Kosterlitz–Thouless transition temperatures (T_{KT}; see text) on n for the two polarization states; the dotted line is a guide to the eye to highlight the linear relationship. Values of n are obtained from the high temperature Hall coefficient values. The T_c criteria (T_c^{a-c} and $T_{KT}^{d,e}$) and the values for the two polarization states are as follows. T_c^a, the temperature at which the resistivity decreases to 50% of that at 400 mK, that is, Beasley's criterion (P+ and P−, 236 mK and 296 mK); T_c^b, the mean field transition temperature determined by fitting the bottom part of the resistivity curves[21] (239 mK, 295 mK); T_c^c, the mean field transition temperature determined by fitting the onset of the transitions with a 2D fluctuation model (240 mK, 298 mK); T_{KT}^d, the temperature at which the resistivity decreases to 1% of that at 400 mK, that is, Beasley's criterion for T_{KT} (181 mK, 272 mK); T_{KT}^d, the KT transition temperature determined by fitting the bottom part of resistivity curves[21] (170 mK, 252 mK). The error bars on T_c and T_{KT} result from uncertainties on the fitting. The maximum error is estimated to be about 10 mK. The error bars on n correspond to the observed small variations in the Hall coefficient at high temperatures.

the well known (but yet to be understood) bell-shape T_c phase diagram illustrated by the dotted and dashed lines in Fig. 4a.

In conclusion, we have achieved large ferroelectric field effects using a model system device based on thin films of PZT and Nb-STO. Large modulations of the resistivity, inverse Hall coefficient and 2D superconductivity are obtained. At a given temperature, complete switching from the normal state to a zero resistance superconducting state upon reversal of the PZT polarization direction is observed, an effect that represents a new step towards nanoscale electronic devices.

METHODS

Heterostructures. Epitaxial heterostructures composed of 500-Å-thick PZT and 260-Å-thick Nb-STO were fabricated on TiO_2-terminated (001) STO single-crystal substrates.

Nb-STO layer deposition. A pulsed laser deposition method employing KrF excimer laser pulses (100 mJ) focused on a commercial 1 wt% (2 atm%) Nb-doped $SrTiO_3$ single-crystal target was used. During deposition, the substrate temperature was kept between 1,200 and 1,300 °C and the oxygen pressure between 2×10^{-7} and 2×10^{-6} torr. In order to get conductive films, high substrate temperature and low oxygen pressure during the deposition turned out to be necessary. An infrared (807 nm) diode laser was used to reach the required high substrate temperature, illuminating the substrate from outside the ultra-high-vacuum chamber through a view port[24]. By monitoring the intensity of reflection high-energy electron diffraction (RHEED) during the deposition, step-flow type growth was observed. No particles were observed even in large areas (typically $5 \times 5\,\mu m^2$), a clear advantage for the subsequent growth of high quality epitaxial PZT. After deposition, the films were cooled in 760 torr of oxygen to avoid reducing the film and the substrate.

PZT layer deposition. This layer was deposited by off-axis radio frequency magnetron sputtering in an argon–oxygen flow ($Ar:O_2 = 3:1$) at a total pressure of 0.18 torr and at a substrate temperature of ~500 °C. From X-ray diffraction analyses of these bilayers, the PZT layers are found to be *c*-axis oriented and single-crystal like.

Ferroelectric polarization. To switch the direction of the ferroelectric polarization (parallel or anti-parallel to the *c* axis), a constant voltage of +12 V or −12 V, leading to a field that is larger than the coercive field of PZT, was applied between the tip and the Nb-STO layer. To determine the ferroelectric domain structure, the AFM piezoresponse imaging mode was used. In this mode, the PZT layer is subjected to an a.c. (10 kHz) applied field (1.5 V) and the local linear piezoelectric response is measured with lock-in detection. The sign of the piezoelectric deformation reveals the sign of the ferroelectric polarization. In Fig. 1c, the dark and light red correspond to each sign of the ferroelectric polarization. During the transport measurements, there was no application of any gate voltage, making the device insensitive to possible leakage currents.

Received 11 October 2005; accepted 16 March 2006.

1. Bednorz, J. G. & Müller, K. A. Possible high-T_c superconductivity in the Ba-La-Cu-O system. *Z. Phys. B* **64,** 189–193 (1986).
2. Tokura, Y. (ed.) *Advances in Condensed Matter Science* Vol. 2, *Colossal Magnetoresistive Oxides* (Gordon and Breach, London, 2000).
3. Ahn, C. H., Triscone, J.-M. & Mannhart, J. Electric field effect in correlated oxide systems. *Nature* **424,** 1015–1018 (2003).
4. Schooley, J. F., Hosler, W. R. & Cohen, M. L. Superconductivity in semiconducting $SrTiO_3$. *Phys. Rev. Lett.* **12,** 474–475 (1964).
5. Pfeiffer, E. R. & Schooley, J. F. Superconducting transition temperatures of Nb-doped $SrTiO_3$. *Phys. Lett. A* **29,** 589–590 (1969).
6. Koonce, C. S., Cohen, M. L., Schooley, J. F., Hosler, W. R. & Pfeiffer, E. R. Superconducting transition temperatures of semiconducting $SrTiO_3$. *Phys. Rev.* **163,** 380–390 (1967).
7. Ahn, C. H. *et al.* Local, nonvolatile electronic writing of epitaxial $Pb(Zr_{0.52}Ti_{0.48})O_3/SrRuO_3$ heterostructures. *Science* **276,** 1100–1103 (1997).
8. Takahashi, K. S. *et al.* Electrostatic modulation of the electronic properties of Nb-doped $SrTiO_3$ superconducting films. *Appl. Phys. Lett.* **84,** 1722–1724 (2004).
9. Müller, K. A. & Burkard, H. $SrTiO_3$: An intrinsic quantum para-electric below 4 K. *Phys. Rev. B* **19,** 3593–3602 (1979).
10. Tufte, O. N. & Chapman, P. W. Electron mobility in semiconducting strontium titanate. *Phys. Rev.* **155,** 796–802 (1967).
11. Aidam, R., Fuchs, D. & Schneider, R. Ferroelectric field effect in $YBa_2Cu_3O_{7-\delta}$ thin films. *Physica C* **328,** 21–30 (1999).
12. Lee, C., Destry, J. & Brebner, J. L. Optical absorption and transport in semiconducting $SrTiO_3$. *Phys. Rev. B* **11,** 2299–2309 (1975).
13. Leitner, A. *et al.* Pulsed laser deposition of superconducting Nb-doped strontium titanate thin films. *Appl. Phys. Lett.* **72,** 3065–3067 (1998).
14. Ahn, C. H. *et al.* Electrostatic modulation of superconductivity in ultrathin $GdBa_2Cu_3O_{7-x}$ films. *Science* **284,** 1152–1155 (1999).
15. Cassinese, A., Luca, G. M. D., Prigiobbo, A., Salluzzo, M. & Vaglio, R. Field-effect tuning of carrier density in $Nd_{1.2}Ba_{1.8}Cu_3O_y$ thin films. *Appl. Phys. Lett.* **84,** 3933–3935 (2004).
16. Parendo, K. A. *et al.* Electrostatic tuning of the superconductor-insulator transition in two dimensions. *Phys. Rev. Lett.* **94,** 197004 (2005).
17. Werthamer, N. R., Helfand, E. & Hohenberg, P. C. Temperature and purity dependence of superconducting critical field H_{c2}. III. Electron spin and spin-orbit effects. *Phys. Rev.* **147,** 295–302 (1966).
18. Takahashi, K. S. *et al.* Epitaxial growth and transport properties of Nb-doped $SrTiO_3$ thin films. *Proc. SPIE* **5932,** 267–274 (2005).
19. Tinkham, M. *Introduction to Superconductivity* 2nd edn (McGraw-Hill, New York, 1996).
20. Kosterlitz, J. M. & Thouless, D. J. Long range order and metastability in two dimensional solids and superfluids. *J. Phys. C* **5,** L124–L126 (1972).
21. Minnhagen, P. The two-dimensional Coulomb gas, vortex unbinding, and superfluid-superconducting films. *Rev. Mod. Phys.* **59,** 1001–1066 (1987).
22. Beasley, M. R., Mooji, J. E. & Orlando, T. P. Possibility of vortex-antivortex pair dissociation in two-dimensional superconductors. *Phys. Rev. Lett.* **42,** 1165–1168 (1979).
23. Gabay, M. & Kapitulnik, A. Vortex-antivortex crystallization in thin superconducting and superfluid films. *Phys. Rev. Lett.* **71,** 2138–2141 (1993).
24. Ohashi, S. *et al.* Compact laser molecular beam epitaxy system using laser heating of substrate for oxide film growth. *Rev. Sci. Instrum.* **70,** 178–183 (1999).

Acknowledgements We thank M. Dawber for a careful reading of the manuscript. This work was supported by the Swiss National Science Foundation through the National Center of Competence in Research, 'Materials with Novel Electronic Properties, MaNEP' and division II, New Energy and Industrial Technology Development Organization (NEDO) of Japan, and ESF (Thiox).

Author Information Reprints and permissions information is available at npg.nature.com/reprintsandpermissions. The authors declare no competing financial interests. Correspondence and requests for materials should be addressed to J.-M.T. (Jean-Marc.Triscone@physics.unige.ch).